POLITECNICO DI TORINO
Repository ISTITUZIONALE

Simulation of secondary flows in turbomachinery by the discontinuous Galerkin method

(Article begins on next page)

07 April 2025

Simulation of Secondary Flows in Turbomachinery by the Discontinuous Galerkin Method

Michele Errante[1,a)], Andrea Ferrero[1,b)] and Francesco Larocca[1,c)]

[1]*Department of Mechanical and Aerospace Engineering (DIMEAS)*
Politecnico di Torino, Italy
Corso Duca degli Abruzzi, 24 - 10129 Torino, Italy

[a)]michele.errante@polito.it
[b)]andrea_ferrero@polito.it
[c)]francesco.larocca@polito.it

Abstract. Secondary flows have a huge impact on low pressure turbines losses. For this reason, several experimental and numerical works have been carried out with the purpose of studying the phenomenon and its effects. The present work aims at investigating secondary flows in a linear low-pressure turbine cascade performing RANS analyses by means of a CFD code based on a Discontinuous Galerkin method, developed by the aerospace propulsion research group (DIMEAS) at Politecnico di Torino. The peculiarities of the flow field within the cascade passage are discussed. Comparisons between the results obtained and those presented in other experimental and numerical works show that the investigations are considered to be valid.

INTRODUCTION

Contrary to what might be deduced from the adjective "secondary", the influence of secondary flows over the entire turbine cascade passage flow field is an issue of paramount importance. In low-pressure turbines (LPTs) the set of complex three-dimensional vortex structures, originated from the interaction between the incoming end-wall boundary layer and the cascade, is responsible for about 40% of total losses. For this reason in the last decades a great number of experimental and numerical studies has been carried out with the purpose of better understanding the phenomenon, to correctly estimate its effects.

In the current work, RANS analyses are carried out to study secondary flows in the T106 LPT linear cascade by means of a CFD code based on the discontinuous Galerkin method. Focus is put on the secondary flows structures, their influence on the blade load variation along the span and the flow field evolution downstream of the trailing edge.

PHYSICAL DOMAIN

A highly loaded low-pressure turbine cascade was chosen for the investigations. In particular, the blade profile selected is the T106A. This configuration consists of a chord to axial chord ratio of 1.164, a pitch to axial chord ratio of 0.929, a span to axial chord ratio of 2.206 and an inlet flow angle of 127.7 deg with respect to the pitchwise direction. Since the calculations are carried out using non-dimensional quantities, all geometric specifications are scaled with respect to the axial chord c_x. The Reynolds and Mach numbers were chosen according to the experimental study of Duden and Fottner [1] and the numerical work of Pichler *et al.* [7] and Marconcini *et al.* [8], $Re = 120000$ and $M = 0.59$.

In the computational domain built for the RANS analysis, x, y and z are the axial, spanwise and pitchwise directions, respectively. The leading edge is located at x = 0, the inlet is at x = -0,8 and the outlet is at x = 2, hence the total axial extension of the domain is set equal to 2.8 times the blade axial chord. Since the flow field is expected to be symmetrical with respect to the midspan plane, the spanwise extension of the domain is exactly equal to half of the span dimension. At the midspan surface, located at y = 0, the flow tangency condition is imposed. In order to simulate

a linear cascade, a periodic condition is used to connect the faces located at the pitchwise domain boundary. On the inlet section uniform conditions were set, hence simulations are conducted without inlet boundary layer.

NUMERICAL SET-UP

A R&D code [2], developed by the aerospace propulsion research group (DIMEAS) at Politecnico di Torino, was used in order to perform the RANS investigations. The code solves the unsteady, three-dimensional, Reynolds-averaged Navier-Stokes equations in a discontinuous finite elements formulation, based on the Discontinuous Galerkin method. Convective fluxes are discretized implementing the Osher flux, proposed by Osherand and Solomon [3], following the approach presented by Pandolfi [4]. Moreover the Enhanced Stability Recovery (ESR) approach proposed by Ferrero, Larocca, and Puppo [5] is adopted for computing diffusive fluxes.

  The closing model chosen for RANS equations is the Spalart-Allmaras (SA) turbulence model, in the version described by Allmaras, Johnson, and Spalart [6]. The scheme selected for computations is second order accurate in space, and besides, for time discratization the implicit backward Euler scheme is used.

  The spatial domain is discretized using a multi-block grid assembled by an O-type structured grid around the blade profile and a non structured grid for the remaining domain, for a total of about 2.4 million cells. Particular attention was paid to the size of elements close to the blade and in proximity of the end-wall, to ensure adequate spatial resolution for both the boundary layer and aerodynamic structures constituting the secondary flows.

RESULTS

Streamlines

The most immediate way to visualize the aerodynamic structures that constitute the secondary flows is to observe the evolution of the current lines within the cascade passage. Figure 1 shows only those streamlines on the inlet section that cover 15% of the spanwise extent of the domain, i.e. 5.5% of the whole span lenght. Downstream of the trailing edge two vortices are clearly recognisable close to the suction side: the passage vortex (P) and the counter vortex (CV), which stays above P and counterrotates against it.
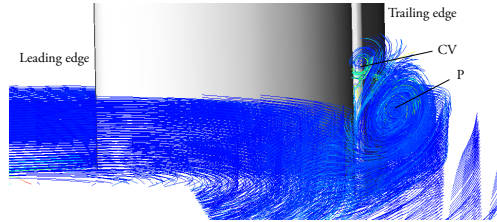

FIGURE 1. Streamlines within the cascade passage.

Pressure distribution

The evaluation of the pressure distribution provides a very clear idea of the effects of secondary flows on the blade load variation along the span. It is defined as:

$$c_p = \frac{p(x) - p_{out}}{p_{in}^\circ - p_{out}} \tag{1}$$

where p_{in}° is the freestream stagnation pressure at the inlet and p_{out} is the mass-average static pressure at the outlet. Referring to Figure 2, it can be seen that moving from the midspan plane towards the endwall surface, the flow does not experience substantial variations in terms of pressure on the suction side, contrary to what occurs on the pressure side. This is reflected in a reduction of lift generated by the blade as the endwall is approached from midspan, since the area between the suction and pressure side pressure distribution visibly decreases. The reason lies in the presence of the endwall cross flow which moves the vortex structures of secondary flows from the suction to the pressure side.
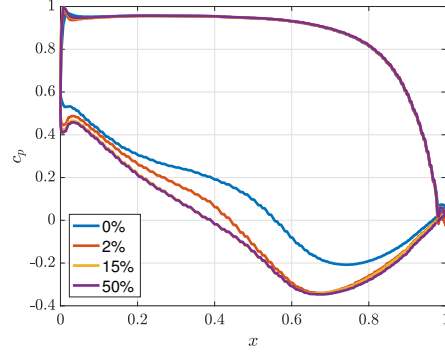
FIGURE 2. Pressure distribution around the blade at different spanwise locations.

Decay of the secondary flow vortices downstream of the trailing edge

Figure 3 illustrates the mass-averaged flow angle β evolution downstream of the blade trailing edge. The peculiar pattern of a turbine cascade is visible: an overturning of the flow in proximity of the endwall followed by an underturning as the distance from the midspan decreases. This phenomenon reflects the presence of secondary flow structures. Since the intensity of those vortices is reduced far from the trailing edge due to viscous effects, the maximum amount of overturning and underturning shrinks as the flow develops.
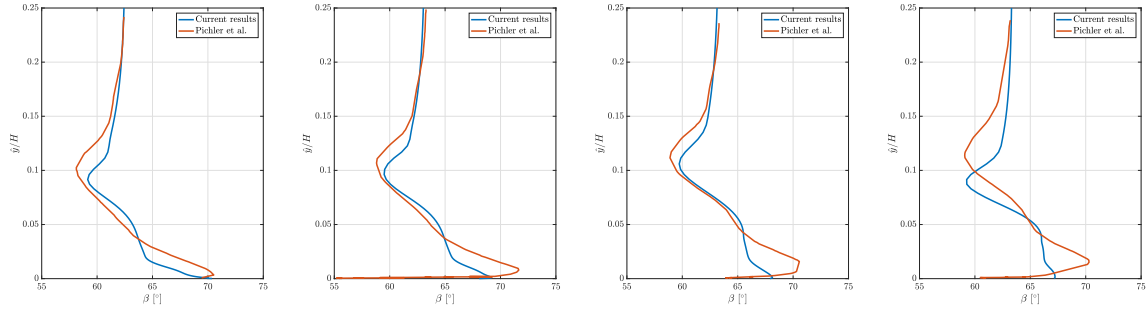

FIGURE 3. Pitchwise averaged flow angle with respect to the axial direction along the spanwise direction at four locations: $x/c_x = 1.03$, $x/c_x = 1.10$, $x/c_x = 1.30$, $x/c_x = 1.50$ (from left to right). The results obtained are compared with the ones presented by Pichler *et al.* [7].
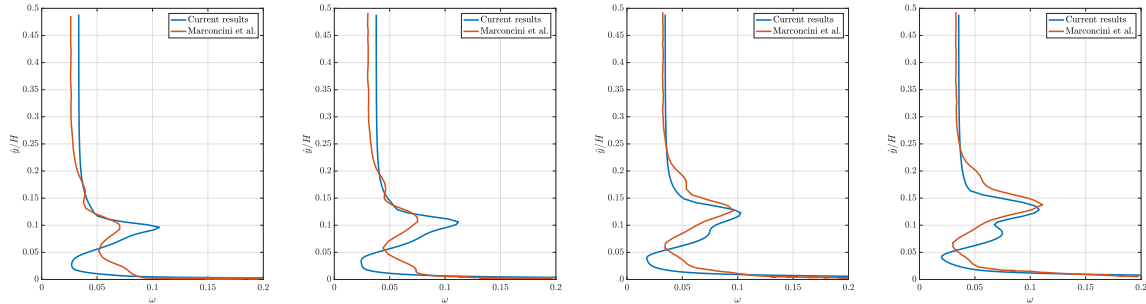

FIGURE 4. Spanwise distributions of total pressure loss coefficient at four axial locations: $x/c_x = 1.03$, $x/c_x = 1.10$, $x/c_x = 1.30$, $x/c_x = 1.50$ (from left to right). The results obtained are compared with the ones presented by Marconcini *et al.* [8].

Figure 4 shows the spanwise distributions of the total pressure loss coefficient ω at different axial locations downstream the trailing edge defined as:

$$\omega = \frac{p_{in}^{\circ} - p^{\circ}}{p_{in}^{\circ} - p}. \tag{2}$$

The calculations were performed by using a mass-averaging. It is evident, at 10% of the span, the contribution of the secontary flows vortices to the global loss. As the flow evolves downstream of the cascade, the ω peak moves towards the midspan due to the influence of the passage vortex and the other vortices. In Figure 3 and 4 the results presented by Pichler *et al.* [7] and Marconcini *et al.* [8] are reported for a comparison. Although they were obtained under different conditions at the inlet, it can be observed that the simulations carried out for the present work correctly captured the physics of the secondary flows and their position in space. Referring to Figure 4, for $x/c_x = 1.30$ and $x/c_x = 1.50$, not only do the curves share the same trend, the absolute values of the loss coefficient are also very close, as the axial locations are far from the trailing edge and the flow is less affected by the presence of the passage vortex.
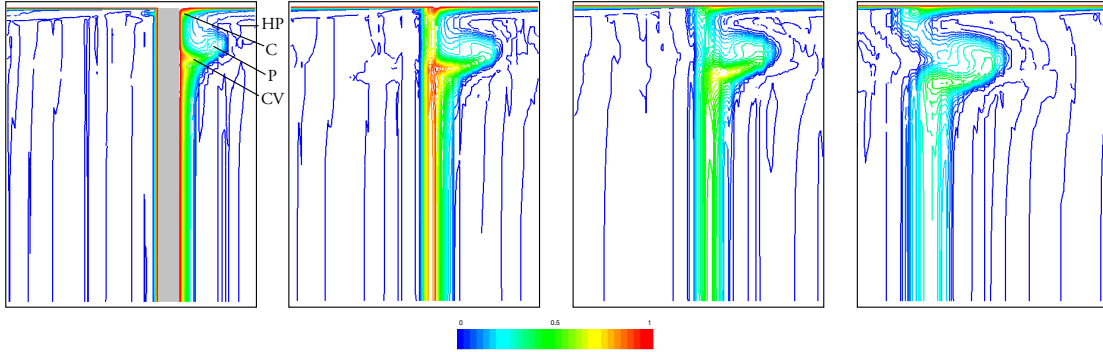

FIGURE 5. Loss coefficient ω contours at $x/c_x = 0.90$, $x/c_x = 1.03$, $x/c_x = 1.10$, $x/c_x = 1.30$ (from left to right).

The losses generated by the secondary flows can be analyzed also by plotting the 2D loss coefficient contours in various axial locations (Figure 5). The pattern of the distribution shows the so called "dog-bone" geometry, typical for highly loaded turbine cascades. It is possible to distinguish the vortices which produces more losses, such as the passage vortex, the corner vortex, the pressure side leg of the horseshoe vortex and the counter vortex, indicated by the labels P, C, HP and CV, respectively.

ACKNOWLEDGMENTS

REFERENCES

[1] A. Duden and L. Fottner, Proceedings of the Institution of Mechanical Engineers, Part A: Journal of Power and Energy **211**, 309–320 (1997).
[2] A. Ferrero, "Computational fluid dynamics for aerospace propulsion systems: an approach based on discontinuous finite elements," Ph.D. thesis, Politecnico di Torino 2015.
[3] S. Osherand and F. Solomon, Mathematics of Computation - Math. Comput. **38** (1982).
[4] M. Pandolfi, AIAA Journal **22** (1984).
[5] A. Ferrero, F. Larocca, and G. Puppo, International Journal for Numerical Methods in Fluids **77** (2015).
[6] S. Allmaras, F. Johnson, and P. Spalart, Seventh International Conference on Computational Fluid Dynamics (ICCFD7), Big Island, Hawaii (9-13 July 2012).
[7] R. Pichler, Y. Zhao, R. Sandberg, V. Michelassi, R. Pacciani, M. Marconcini, and A. Arnone, Journal of Turbomachinery **141** (2019).
[8] M. Marconcini, R. Pacciani, A. Arnone, V. Michelassi, R. Pichler, Y. Zhao, and R. Sandberg, Journal of Turbomachinery **141** (2019).